

**MODELLING INTERACTION BETWEEN WAVES AND SEAWALLS  
USING A NUMERICAL WAVE FLUME**

**N.Q. Chien<sup>1</sup> and T.T. Tung<sup>1</sup>**

**Abstract:** Numerical wave flumes are useful in predicting detailed flow patterns due to wave breaking in the surf zone, which is very important in design of coastal structures. In this study, the CADMAS-SURF model (2001) is used to get insight into cross-shore wave and flow processes in the surf zone, and to some extent, to evaluate the impact of waves to a typical seawall in Vietnam. The model is first verified against Suzuki's (2011) laboratory-scaled experiment, then against a field survey on a barred beach (Eldeberky 2011). The tuneable parameters include porosity of the seabed layer, drag coefficient, and inertia coefficient of the flow in this layer. As CADMAS-SURF includes a k-epsilon turbulence model, certain wave parameters e.g. wave breaking and dissipation do not need to be specified. Simulation is then performed for extreme wave conditions offshore Do-Son beach (Vietnam). Storm waves and water levels are chosen for annual exceedance probabilities of 1%, 3.33%, and 5%. The simulation outputs including water surface profile, wave heights, flow-, and pressure-fields are summarized to show possibly severe impacts on various parts: toe, slope, and crest of the structure.

**Keywords:** numerical wave flume; wave hydrodynamics; wave-structure interaction; seawall; Vietnam.

**1. INTRODUCTION**

For designing or evaluating performance of coastal structures, numerical wave flumes (NWF) are important tools. An NWF simulation provides flow velocity and pressure fields in the vicinity of the coastal structure, which helps the modeller to identify key structure parts where the wave action is most intense and protection is needed.

The CADMAS-SURF model (CDIT 2001) was

$$\frac{\partial \gamma_x u}{\partial x} + \frac{\partial \gamma_z w}{\partial z} = S_p \tag{1}$$

$$D(\lambda u) = -\frac{\gamma_v}{\rho} \frac{\partial p}{\partial x} + \gamma_v D_x u - R_x + \frac{\partial}{\partial x} \left\{ \gamma_x v_e \left( 2 \frac{\partial u}{\partial x} \right) \right\} + \frac{\partial}{\partial z} \left\{ \gamma_z v_e \left( \frac{\partial u}{\partial z} + \frac{\partial w}{\partial x} \right) \right\} + \gamma_v S_u \tag{2}$$

$$D(\lambda w) = -\frac{\gamma_v}{\rho} \frac{\partial p}{\partial z} + \gamma_v D_z w - R_z + \frac{\partial}{\partial z} \left\{ \gamma_z v_e \left( 2 \frac{\partial w}{\partial z} \right) \right\} + \frac{\partial}{\partial x} \left\{ \gamma_x v_e \left( \frac{\partial w}{\partial x} + \frac{\partial u}{\partial z} \right) \right\} + \gamma_v S_w + \gamma_v g \tag{3}$$

in which  $\gamma_v$ ,  $\gamma_x$ ,  $\gamma_z$  are the volume porosity and surface permeability in  $x$ - and  $z$ -directions, respectively;  $\lambda_v$ ,  $\lambda_x$ ,  $\lambda_z$  are the corresponding coefficients with inertia factor ( $C_M$ ) taken into account,  $\lambda = \gamma + (1 - \gamma) C_M$ , whereas

originally developed to study wave-structure interaction, especially wave impact on coastal structures. The model is based on Reynolds-Averaged Navier-Stokes (RANS) equations, which adequately describe the behaviour of unsteady, turbulent, viscous fluid flows. For a 2-D version of the model used in this study, the equations read:

$D(\lambda \bullet) = \lambda_v \frac{\partial \bullet}{\partial t} + \frac{\partial \lambda_x u \bullet}{\partial x} + \frac{\partial \lambda_z w \bullet}{\partial z}$  is the total derivation of the velocity component ( $\bullet$ ),  $D_x$  and  $D_z$  are the coefficients of energy dissipation,  $v_e$  is the eddy viscosity;  $S_p$ ,  $S_u$ , and  $S_w$  are source terms associated with wave generation;  $R_x$  and  $R_z$  are the

<sup>1</sup> Faculty of Coastal Engineering, Thuyloi University

resistant forces from the porous structure:

$$R_x = \frac{1}{2} \frac{C_D}{\Delta x} (1 - \gamma_x) u \sqrt{u^2 + w^2} \quad (4)$$

$$R_z = \frac{1}{2} \frac{C_D}{\Delta z} (1 - \gamma_z) w \sqrt{u^2 + w^2} \quad (5)$$

The computational domain is discretized on rectangular grids, where each grid cell holds information regarding fluid velocity vector ( $\mathbf{u}$ ) and pressure ( $p$ ).

To model the fluid-structure interaction, the water surface must be correctly delineated. An effective method is Volume-of-Fluid (VoF) (Hirt and Nichols 1981), where the volume of fluid in each grid cell is tracked using a function  $F$  ( $F = 0$  or 1 represents the cell is fully occupied by air or water,

$$D(\lambda k) = \nabla^2 (\gamma v_k k) + \gamma_v (G_S + G_T - \varepsilon) \quad (7)$$

$$D(\lambda \varepsilon) = \nabla^2 (\gamma v_\varepsilon \varepsilon) + \gamma_v \left\{ C_1 \frac{\varepsilon}{k} (G_S + G_T) (1 + C_3 R_f) - C_2 \frac{\varepsilon^2}{k} \right\} \quad (8)$$

where  $G_S$  is related to velocity strains,  $G_T$  – to buoyancy, and  $R_f = G_T / (G_S + G_T)$  (Suzuki 2011). The coefficients are generally taken as  $C_1 = 1.44$ ,  $C_2 = 1.92$ ,  $C_3 = 0$ ,  $C_\mu = 0.09$ ,  $\sigma_k = 1$ , and  $\sigma_\varepsilon = 1.3$ , which are the default values for the standard  $k$ - $\varepsilon$  model developed by Launder and Spalding (1974).

## 2. MODEL VERIFICATION

### 2.1. Against Suzuki's (2011) experiment

Suzuki (2011) conducted experiment on a scale model representing a synthetic coastal profile with a short slope (1/4.7) followed by a longer gentle slope (1/20.5) (Fig. 1). The water depth at the seaward boundary was 0.375 m and the incident waves were regular with period  $T = 1.6$  s. Three scenarios were considered with wave heights  $H_i = 5.4$  cm, 7.4 cm, and 11.0 cm.

The computation grid comprises  $600 \times 120$  cells, with grid spacings  $\Delta x = 2$  cm and  $\Delta z = 0.5$  cm. By specifying so, each wave height can be vertically resolved within at least 10 grid cells and each wave length – 80 grid cells (Hanzawa et al. 2012). An adaptive time step has been automatically chosen; for this case  $\Delta t$  appears to be in the range from 0.0065 s to 0.0066 s.

respectively). The advection equation for  $F$  is:

$$\gamma_v \frac{\partial F}{\partial t} + \frac{\partial \gamma_x u F}{\partial x} + \frac{\partial \gamma_z w F}{\partial z} = \gamma_v S_F \quad (6)$$

In addition, a predefined index (NF) is chosen for each cell to indicate how the air-water interface cuts through the cell. This VoF-based model is suitable for simulating complex waves deformation, e.g. plunging, in the surf zone.

The donor-acceptor technique is used to compute the advection term in Eq. (6); this helps to limit the flux between cells close to the surface.

The turbulence model is  $k$ - $\varepsilon$  type where the kinetic energy,  $k$ , and rate of energy dissipation,  $\varepsilon$ , are described by the following equations:

In this simulation, no porous structure presents. The gradually varying bed slope causes waves to dissipate in ‘spilling’ pattern (corresponding to Iribarren number of  $\xi_0 = 0.42$ ).

The waveform and velocity field are shown in Fig. 1. The waves are periodic but not sinusoidal, with sharper crests and flatter troughs. This 5<sup>th</sup> order Stokes waveform is the default option for generating waves at the offshore boundary. The waves become asymmetric from the location  $x = 5$  m shoreward.

The orbital velocity shows that fastest motion occurs under the wave crest during shoaling ( $x = 5.2$  m), incipient breaking ( $x = 7.2$  m), and run-up ( $x = 8.8$  m).

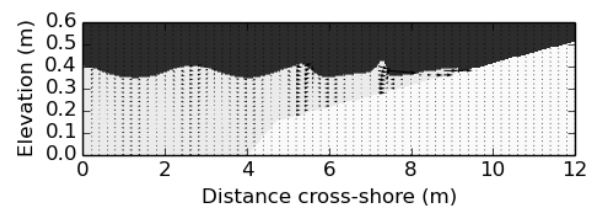


Fig 1. Snapshot of wave form and velocity field for a regular wave ( $H_i = 5.4$  cm) propagating across a synthetic bed profile

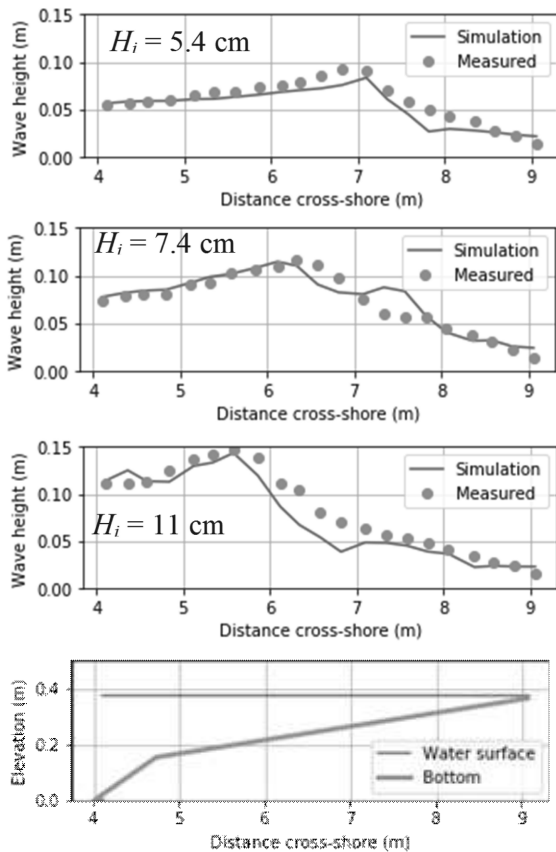


Fig 2. Distribution of wave height across shore for various incident wave heights ( $H_i$ ): comparison between CADMAS-SURF simulation and measured data by Suzuki (2011)

By analysing the time series of water level, the simulated wave height across the bed profile is obtained for three cases of incident wave heights ( $H_i$ ) (Fig. 2). For each case, apparently wave shoaling occurs along halfway of the upper slope, until the wave height reaches a peak, then wave breaking and intense dissipation follows. Also for higher  $H_i$ , wave breaking occurs earlier and further from the shore.

Generally, the cross-shore distribution of simulated wave height has similar trend to that measured. The wave breaking index ( $\gamma$ ) by simulation is approximately 0.78, which matches the theoretical value for regular waves. The difference between computed and measured data mainly occurs in the wave breaking zone, which is likely due to imprecise estimation of the water surface in the complex wave breaking condition.

## 2.2. Against Arcilla et al. (1994)'s experiment

As part of a systematic (benchmark) test case

collection, Arcilla et al. (1994) performed experiments regarding random wave propagation over a barred beach in the Delft Hydraulics' Delta wave flume. The apparatus included a 200-m long profile (Fig. 3, bottom) consisting of two sections: a roughly 1:20 planar slope followed by a concave one. A sand bar (0.4 m high) was located on the concave section. The bed elevation varied from 5 m to 0 m, the still water level was 4.1 m, and the offshore random wave boundary condition is taken as  $H_{m0} = 0.6$  m,  $T_p = 8$  s.

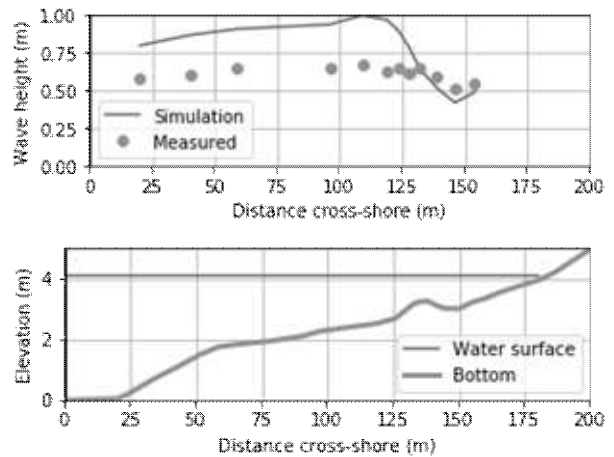


Fig. 3 Cross-shore distribution of wave height: comparison between CADMAS-SURF simulation, measured data (Arcilla et al. 1994), and simulation using a spectral wave model (Eldeberky 2011)

To achieve adequate resolution, the grid spacings  $\Delta x = 0.1$  m and  $\Delta z = 0.05$  m are chosen.

In-situ beach sand is considered as a porous material with  $\gamma_v = 0.4$ . The transmittance coefficients are chosen as  $\gamma_x = \gamma_z = 0.3$ . The non-spherical sand grains (with shape factor generally about 0.7) exhibits a drag coefficient of  $C_D = 1.2$  against turbulent flows. The inertia factor  $C_M$  should be chosen through calibration. Phung et al. (2006) investigated the cross-shore wave height distribution for a range of  $C_M$  from 0.5 to 2.0 (rubble mound with size  $D_m$ :  $H_i/D_m = 3.68$ ), and found that the results vary complicatedly. In the case with sand material, Phung (personal communication) suggested a value of 0.8. Correspondingly,  $\lambda_v = 0.88$ .

The simulated wave height distribution follows the trend of measured data (Fig. 3), although the magnitude does not match well. However, it should be noted that Archilla et al. (1994) used wave gauges with integrated system to post-process wave data and obtained  $H_{m0}$  directly, while the authors used the relationship  $H_{m0} = 4\sqrt{m_0}$ . This simple formula was used in other wave models such as that of Elderberky (2011), but is suitable only for linear waves in deep water; in shallow water the wave spectrum changes therefore the formula is no longer accurate.

This test case shows that, by using CADMAS-SURF, the wave propagation process across a sandy (porous) seabed can be reproduced with reasonable accuracy. The processes of wave shoaling then breaking above the sand bar is apparent.

### 3. APPLICATION TO DO-SON COAST

The northern coast of Vietnam (latitude 18°N to 21.5°N) is home to millions of inhabitants with fast economic development. Although the seawalls had been constructed systematically along Haiphong and Namdinh coasts to protect local residents and infrastructure, recent climate changes with strong typhoons such as the Doksuri in 2017 have caused potential threats and required further improvement in structural design and construction.

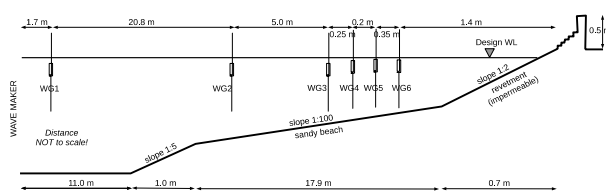


Fig 4. Dimensions of the scale model for a typical profile of Do-Son coast with a stepped seawall. The locations of wave gauges (WG1 to WG6) are shown.

A new pilot project (Research Code TD 145-17) carried out by the Faculty of Marine and Coastal Engineering, Thuyloi University (TLU), in the framework of Vietnam Ministry of Construction aims to improve the sea wall of Do-Son coast (20°40'N, 106°48'E) in Haiphong. A typical coastal profile (Fig. 4) consists of a sandy beach with an average slope of 1:100 followed by an

impermeable revetment (slope 1:2), and then a stepped seawall (Fig. 4).

In this study, the model is established conforming to a hydraulic lab experiment with geometrical scaling of 1:15. The purpose is to verify the results of simulation against that of experiment. However, at present only numerical simulation result is available; the verification is presented in a later study.

### 3.1. Design hydraulic condition

Each design hydraulic condition combine still water depth ( $h$ ), incident wave height ( $H_i$ ), and wave period ( $T$ ), which correspond to an annual exceedance probability  $P$ . The following three conditions are considered, in which figures are scaled from design values:

- $h = 0.70$  m,  $H_i = 0.18$  m,  $T = 2.0$  s ( $P = 1\%$ );
- $h = 0.65$  m,  $H_i = 0.17$  m,  $T = 1.6$  s ( $P = 3.33\%$ );
- $h = 0.60$  m,  $H_i = 0.16$  m,  $T = 1.5$  s ( $P = 5\%$ ).

### 3.2. Model setup and parameters

For this realistic simulation, the grid must be chosen fine enough, to show details of the flow- and pressure-fields at the vicinity of the sea wall. The grid spacings are  $\Delta x = 0.025$  m and  $\Delta z = 0.01$  m. The size of each step on the seawall is equivalent to one cell.

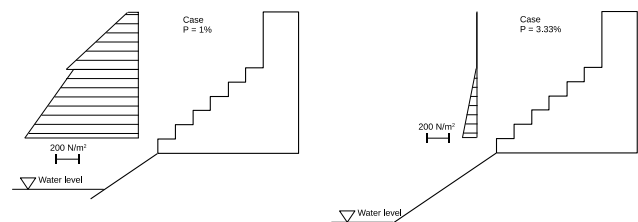
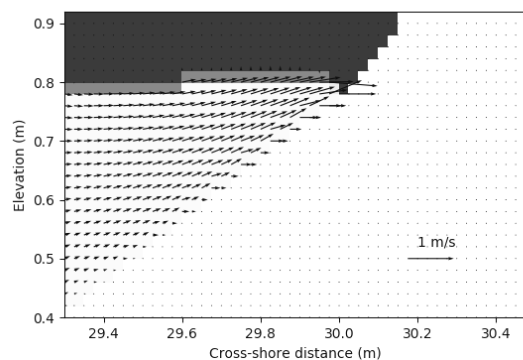


Fig 5. Distribution of maximum pressure on the stepped seawall



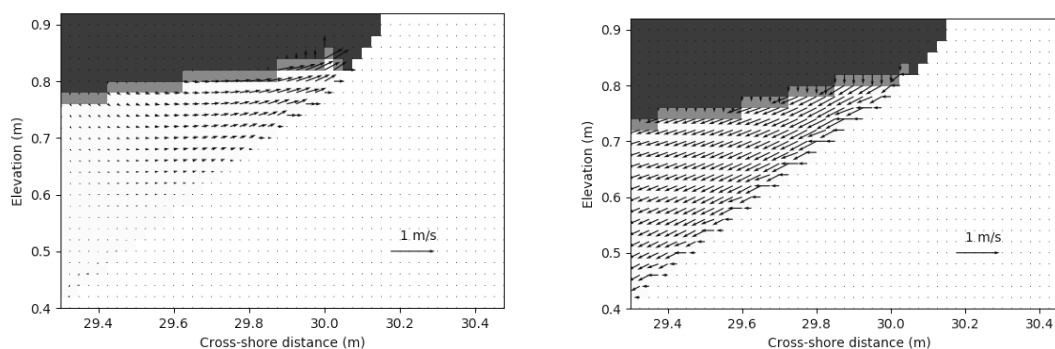


Fig 6. Flow field close to the revetment during various phases of incoming wave

### 3.3. Simulation result

The simulation time period is 120 s. It takes about 60 s for the system to reach almost equilibrium. Table 1 represents the wave height variation from intermediate depth (WG1) to shallow water zone (WG6), for three scenarios.

**Table 1. Wave height at locations indicated on Fig. 4**

Location	Scenarios		
	$P = 1\%$	$P = 3.33\%$	$P = 5\%$
WG1	0.210 m	0.213 m	0.138 m
WG2	0.133 m	0.134 m	0.151 m
WG3	0.216 m	0.130 m	0.119 m
WG4	0.161 m	0.141 m	0.115 m
WG5	0.113 m	0.185 m	0.142 m
WG6	0.125 m	0.173 m	0.165 m

The distribution of temporal maximum pressure on the seawall is shown in Fig. 5. Apparently, the waves in case  $P = 1\%$  may have remarkable impacts on the seawall. For the case  $P = 5\%$  the impact is negligible and not shown here.

The velocity field adjacent to the revetment is shown in Fig. 6. The upper subfigure shows dominant wave run-up when the wave crest approaches the structure. The lower left subfigure corresponds to highest run-up, but the uprush flow velocity decreases. In the lower right subfigure, the water surface lowers and induced a steep slope, causing dominant wave run-down.

### 3.4. Discussion

Although NWF provides simulation result in finer detail, the fact that wave transformation undergoes various processes such as shoaling and wave breaking. At WG1 the wave shoaling is prominent for Cases '1%' and '3.33%' but early incipient wave breaking causes the wave height to decrease (which is apparent at WG2). Then waves reform and due to larger water depths of cases

'1%' and '3.33%' at WG3, wave heights are greater than that of case '5%'.

The capability of CADMAS-SURF to produce detailed flow- and pressure-fields is important to evaluate the performance of coastal structure. However a higher grid resolution is required to represent highly turbulent flows.

Further verification needs to be carried out regarding flow velocity, especially the fluid layer close to seabed. A first impression on the velocity field between the fluid and porous media is that there is a change in flow direction at this interface. The flow velocity is not necessarily smaller in the porous medium. In some situations this might be harmful to the structure as reverse pressure is formed.

### 4. CONCLUSION

Numerical wave flumes (NWF) such as CADMAS-SURF have been proven to be useful in simulation and helps evaluate the performance of structures. Certain simulation cases have been carried out to verify the model against measured data from literature, namely:

- wave propagation toward and breaking on an impermeable slope;
- wave propagation and dissipation on a natural barred beach.

The computed wave heights match reasonably well with data, except for a section immediately after incipient wave breaking.

The model is then used to simulate wave impact on a cross-section of the seawall at Do-Son, Haiphong, Vietnam. The highest pressure on the seawall is presented in Case '1%'. For this case, even some overtopping is expected.

For simulations involving wave-structure interaction, the standard set of parameters for  $k$ - $\epsilon$  model can be adopted. The porous material is specified in terms of void fraction,  $\gamma_v$ , the transmittance coefficients,  $\gamma_x$  and  $\gamma_z$ , the drag

coefficient  $C_D$ , and the inertia factor  $C_M$ . With an appropriate choice for the above parameters, NWF is a good tool, which can provide an overall picture of wave propagation and interaction with structure. On the other hand, results obtained from an NWF simulation need to be analysed.

#### ACKNOWLEDGEMENTS

This study is conducted as part of the Project

“Research on manufacturing of seawall units with return wall, for protection urban, resort and island shorelines” (Research Code TD 145-17), funded by Ministry of Construction, Vietnam.

The authors thank Coastal Development Institute of Technology, Japan, for releasing CADMAS-SURF V5.1 as open-source software.

#### REFERENCES

- Arcilla, A.S., Roelvink, J.A., O'Connor B.A., and Jimenez, J.A. (1994). *The Delta flume '93 experiment*. Proc. Int. Coastal Dynamics Conf. Barcelona: 488–502.
- Coastal Development Institute of Technology (2001). *Research and development of numerical wave flume “CADMAS-SURF” (in Japanese)*, 457 pp.
- Eldeberky, Y. (2011). *Modeling spectra of breaking waves propagating over a beach*. Ain Shams Eng. J. 2: 71–77.
- Hanzawa, M., Matsumoto, A. and Tanaka, H. (2012). *Applicability of CADMAS-SURF to evaluate detached breakwater effects on solitary tsunami wave reduction*. Earth Planet Space 64: 955–964.
- Hirt, C.W. and Nichols, B.D. (1981). *Volume of fluid (VOF) method for the dynamics of free bodies*. J. Comput. Phys. 39: 201–225.
- Lauder, B.E. and Spalding, D.B. (1974). *The numerical computation of turbulent flows*. Comput. Meth. Appl. M. 3(2): 269–289.
- Phung, D.H. and Tanimoto, K. (2006). *Verification of a VOF-based two-phase flow model for wave breaking and wave-structure interactions*. Ocean Eng. 33: 1565–1588.
- Phung, D.H. and Pham, N.V. (2012). *Numerical study of wave overtopping of a seawall supported by porous structures*. Appl. Math. Modell. 36: 2803–2813.
- Suzuki, T. (2011). *Wave dissipation over vegetation fields*. PhD thesis, TU Delft.

#### Tóm tắt:

### MÔ HÌNH HOÁ TƯƠNG TÁC SÓNG - TƯỜNG BIỂN BẰNG MẢNG SÓNG SỐ

Mảng sóng số là công cụ hữu ích để ước tính trường dòng chảy chi tiết gây ra bởi sóng vỡ vùng ven bờ, vốn rất quan trọng trong việc thiết kế công trình bờ biển. Nghiên cứu này sử dụng mô hình CADMAS-SURF (2001) để tìm hiểu các quá trình sóng và dòng chảy ngang bờ trong vùng sóng vỡ, và một phần xác định lực tác động của sóng lên công trình tường biển, điển hình ở Việt Nam. Trước hết, mô hình được kiểm định theo thí nghiệm do Suzuki (2011) thực hiện, sau đó là kiểm định theo kết quả đo đạc hiện trường với bãi biển có dải đảo chắn (Eldeberky 2011). Các tham số hiệu chỉnh được bao gồm độ rỗng lớp đáy biển, hệ số cản, và hệ số quán tính của dòng chảy trong lớp này. Do CADMAS-SURF đã bao gồm một mô hình rối  $k$ -epsilon, nên không cần quy định một vài tham số liên quan đến sóng vỡ và tiêu tán năng lượng sóng. Tiếp theo, mô phỏng được thực hiện cho các điều kiện sóng cực trị cho vùng ngoài biển Đồ Sơn (Việt Nam). Sóng và mực nước dâng trong bão đã được chọn cho các tần suất vượt 1%, 3.33%, và 5%. Kết quả mô phỏng bao gồm dạng đường mặt nước, chiều cao sóng, cũng như trường dòng chảy được tổng hợp lại, từ đó cho thấy những tác động phá hoại có thể xảy ra tới chân, mái, và đỉnh công trình.

**Từ khóa:** mảng sóng số; động lực sóng; tương tác sóng – công trình; tường biển; Việt Nam.

---

Ngày nhận bài: 28/8/2019

Ngày chấp nhận đăng: 01/10/2019